COBEM 2023 27TH INTERNATIONAL CONGRESS OF MECHANICAL ENGENEERING

ABCM Brazilian Society of Mechanical Sciences and Engineering
27th ABCM International Congress of Mechanical Engineering
December 04-08, 2023, Florianópolis-SC, Brazil

COB-2023-0732
AN EFFICIENCY STUDY FOR AN SOFC SYSTEM USING ETHANOL AND LUMPED MODELS

Igor Silva Flores Siqueira
Programa de pós-Graduação em Engenharia e Ciências Mecânicas – Universidade Federal de Santa Catarina
Bruno Francisco Oechsler
Programa de pós-Graduação em Engenharia Química – Universidade Federal de Santa Catarina
b.oechsler@ufsc.br

Rafael de Camargo Catapan
Programa de pós-Graduação em Engenharia e Ciências Mecânicas – Universidade Federal de Santa Catarina
rafael.catapan@ufsc.br

Abstract. *The growing demand for energy production and concerns about the environmental impact caused by traditional energy sources have driven research into new and highly efficient strategies in the transportation sector. Most vehicles around the world use fossil fuels, resulting in greenhouse gas emissions in the atmosphere. This scenario motivates the research into more efficient methods. In this work, a solid oxide fuel cell (SOFC) integrated with an ethanol reformer was investigated employing lumped models. The key parameter in the study is the efficiency analysis, performed through lumped and stationary models with emphasis on system behavior representation of SOFC, reformer, and heat exchangers. The results were compared with the literature and experimental data in order to be validated. The preliminary results show that the hypotheses adopted in the models for this study are valid to estimate the main characteristics such as voltage, total losses, power, and efficiency of the fuel cell at different temperatures (873 K to 1073 K). The results were compared with the experimental data, showing a good agreement for voltage at 1073 K and a slight discrepancy for 873 K. The results indicates that for specific conditions, the efficiencies can variate from 42.5% to 62.5% for a study range of 300°C in temperature. A investigation for Air/Ethanol ratio provided a efficiency result of 51% to 36.8%. The system model is able to estimate the efficiency, which confirms the hypothesis of implementing a lumped model to represent the system of interest.*

Keywords: *SOFC, reformer, ethanol, system integration, energy recovery.*

1. INTRODUCTION

The increase in demand for energy production and the concern with the environmental impact caused by the traditional sources of energy has become a driver for research in system efficiencies. In particular, the main propose is to improve the use of energy and minimize the associated impacts on the environment (Kaczmarczyk and Gurgul, 2021; Alhazmi *et al.*, 2021).

Currently, the majority of vehicles worldwide rely on fossil fuels as their primary energy source, leading to the release of greenhouse gas in the atmosphere. The concern with the environment has been reflected in the definition of standards, which becomes a challenge for the combustion engine. In order to meet environmental regulations, some countries has setting a target of no longer sell combustion vehicles after 2050. Thus, the search for more efficient methods of energy generation for vehicles is a growing field of industrial interest (Ma *et al.*, 2021; KELES *et al.*, 2008).

In this context, the fuel cell SOFC has emerged as a promising alternative. Several studies have investigated its potential for power generation, replacing conventional sources such as thermoelectric. Additionally, some studies have focused on the use of SOFC in vehicles with compatible efficiency as electric vehicles (Badur *et al.*, 2018; Zhao and Burke, 2009).The solid oxide fuel cell (SOFC) is an electrochemical device that converts chemical energy directly into electricity through the consumption of hydrogen fuel. The operation of a solid oxide fuel cell (SOFC) requires two input components: hydrogen as the fuel and air as the oxidant. However, hydrogen is a fuel that requires high pressure to be stored which can consume space and requires extra safety features for a vehicular application. One solution to address this challenge is the integration of a steam reformer with a fuel cell system. This configuration enables the use of available and easily stored fuels such as natural gas, ethanol, and other hydrocarbons (O'Hayre *et al.*, 2016).

The main advantages of using fuel cells in Brazil is the accessibility to infrastructure suitable for the use of ethanol. Particularly, Brazil has a well-established and extensive network of gas stations that distribute ethanol. The success of ethanol use can be attributed to the Proalcool program (National Ethanol Program), developed by the government in the 70s to encourage the production and use of ethanol as fuel to reduce the dependence on petroleum, which had high prices

during that period. From 1975 to 1976, which is the start of the program, Brazil produced around 600 million litres. In comparison, the ethanol production in 2015-2016 was about 28 billion litres (BioDieselbr, 2006; FAPESP, 2016).

Nissan presented an electric vehicle based on a SOFC integrated with a reformer in 2016 and ran tests in Brazil and Japan (Ma *et al.*, 2021).The reformer was connected to a tank filled with ethanol, which allowed the car to be filled almost everywhere as ethanol is highly available in the country. According to Nissan, the vehicle can run 600 km with 30L of ethanol, running a battery of 24 kWh (Nissan, 2016). This requirement reinforces the necessity to study the energetic efficiency of the system, allowing for reduction to a better-defined size of components according to the module necessity, which can result in cost and size reduction.

In the last 20 years, the number of papers related to the subject of SOFC has increased with more than 27,000 articles. They are mainly divided into anode material development, experimental models, and simulation models to predict the behavior and the key features of energy production. The fuel cell models will take an important position in the next 20 years, especially because they allow to predict the behavior of these systems in different conditions, helping to understand the effect of parameters in the cell performance results. The SOFC literature is vast and several types of models have been developed, from 0D (lumped) to 3D models tested in a steady state or transient conditions, utilizing different strategies, such as theoretical, semi-empirical, or empirical models (Yang *et al.*, 2020; Cheddie and Munroe, 2007; Wang *et al.*, 2011).

Thus, the objective of the present paper is to investigate the energetic efficiency of a SOFC with an ethanol reformer, using a lumped model to simulate the SOFC cell, while the reformer is simulated by a thermodynamic equilibrium model. This objective will be achieved by the implementation of numerical simulation of solid oxide fuel cell (SOFC) using Python Model and Cantera Library, verifying the results against the literature to validate the results obtained and presenting a sensibility study.

2. SOFC MODELS

Fuel cells are electrochemical devices that convert chemical energy into electrical energy, and include different types. It is similar to a battery that generates energy based on an electrochemical reaction but with the difference that it can work indefinitely as long as fuel.The SOFC cell operates in three parts: anode, electrolyte, and cathode. At the cathode, oxygen is supplied, and it gains electrons to form negatively charged oxygen ions (Kupecki, 2018; Revankar and Majumdar, 2016).

Figure 1 presents the schematic of a SOFC. The hydrogen-rich gas is fed as fuel into the anode side, where it combines with the negatively charged oxygen ions transported through the electrolyte, resulting in the production of water and electrons. (Kupecki, 2018; Revankar and Majumdar, 2016). In the sequence, the SOFC lumped model utilized in this paper.

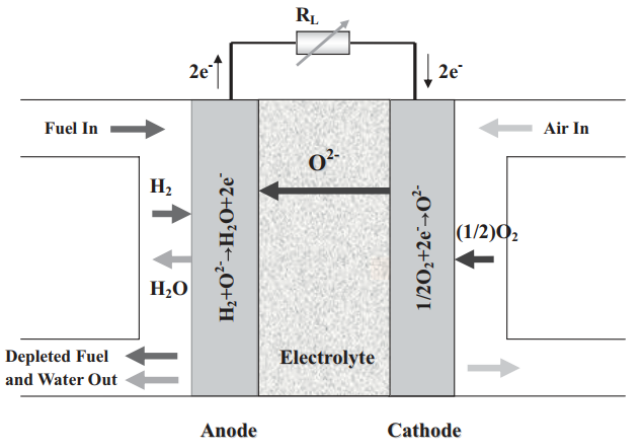

Figure 1. SOFC schematic.
Source:(Chen et al.*, 2010).*

The open circuit voltage $[E_{OCV}]$ for an SOFC is given by the Nerst Equation, which is also called as reversible cell voltage(Saebea *et al.*, 2012), which shows the variation of cell voltages as function of species concentration (O'Hayre *et al.*, 2016).

$$E_{OCV} = E^0 - \frac{RT}{2F} ln\left(\frac{P_{H_2O}}{P_{H_2} P_{O_2}^{0.5}}\right) \tag{1}$$

Where $[E_{OCV}]$ is the open circuit voltage *(V)*, $[R]$ is the constant of gas (J/mol·K), $[T]$ is temperature *(K)*, and

$[P_{H2O}]$,$[P_{H2}]$ and $[P_{O2}]$ the partial pressure of water, hydrogen, oxygen in *(bar)*, and $[E_0]$ is the open circuit voltage (V) at standard pressure, presented in the equation (2):

$$E_0 = 1.253 - 2.4516x10^{-4}T \tag{2}$$

However, in a real condition, the voltage *(V)* is lower than the open circuit voltage $[E_{OCV}]$, because of the irreversible losses in the system. This voltage is given by equation (3), which takes into account the activation loss $[n_{act}]$, ohmic loss $[n_{ohm}]$ and concentration loss which are given in Volts *(V)* $[n_{conc}]$ (Saebea *et al.*, 2012).

$$V = E - \eta_{act} - \eta_{conc} - \eta_{ohm} \tag{3}$$

The ohmic loss, $[n_{ohm}]$, occurs due to the conduction resistance of materials to the flow of electrons through the cell components. This loss is linear with the current density and voltage drop, as presented in equation (4) (Saebea *et al.*, 2012).

$$\eta_{ohm} = jR_{ohm} \tag{4}$$

In which $[R_{ohm}]$ (Ωm^2) is the internal resistance represented by equation (5). The $[\tau_{anode}]$ is the thickness of the anode (μm), $[\sigma_{anode}]$ is the electric conductivity of anode $(\Omega^{-1}m^{-1})$, the same variables for cathode are respectively $[\sigma_{cathode}]$ $(\Omega^{-1}m^{-1})$, $[\tau_{cathode}]$ (μm), and for electrolyte $[\tau_{electrolyte}]$ (μm) ,$[\sigma_{electrolyte}]$ $(\Omega^{-1}m^{-1})$Saebea *et al.* (2012).

$$R_{ohm} = \frac{\tau_{anode}}{\sigma_{anode}} + \frac{\tau_{electrolyte}}{\sigma_{electrolyte}} + \frac{\tau_{cathode}}{\sigma_{cathode}} \tag{5}$$

The concentration loss, $[n_{conc}]$, emerges from the transport limitations within the porous structure of the electrode due to the resistance to the mass transport. It is expressed as the sum of losses in an anode, $[n_{conc,eanode}]$ and in cathode, $[n_{conc,cathode}]$, shown in the following equation as (6), (7) and (8) in Volts (V) (Saebea *et al.*, 2012).

$$\eta_{conc} = \eta_{conc,anode} + \eta_{conc,cathode} \tag{6}$$

$$\eta_{conc,anode} = \frac{RT}{2F} ln\left(\frac{P_{H_2O,TPB}P_{H_2,f}}{P_{H_2O,f}P_{H_2,TPB}}\right) \tag{7}$$

$$\eta_{conc,cathode} = \frac{RT}{2F} ln\left(\frac{P_{O_{2,a}}}{P_{O_{2,TPB}}}\right) \tag{8}$$

$[P_{H2O,TPB}]$ and $[P_{H2,TPB}]$ are the partial pressure at three-phase boundary TPB of water and hydrogen, $[P_{H2f}]$ and $[P_{H2O,f}]$ are the partial pressure in the fuel. The three-phase boundary is a region in which the electrolyte, gas, and electrically phases are in contact, and consequently, reactions occur (O'Hayre *et al.*, 2016).

The partial pressure, $[P_i]$, required to calculate the concentration loss, is determined using Fick's model (Saebea *et al.*, 2012; Arpornwichanop *et al.*, 2009). Equation (9) represents the partial pressure (bar) for the hydrogen in the TPB. Similarly, the Equation (10) represent the partial pressure for water, an equation (11) for oxygen at the same region.

$$P_{H_2,TPB} = P_{H2,f} - \frac{RT\tau_{anode}}{2FD_{eff,anode}} j \tag{9}$$

$$P_{H_2O,TPB} = P_{H_2O,f} - \frac{RT\tau_{anode}}{2FD_{eff,anode}} j \tag{10}$$

$$P_{O_2,TPB} = P - (P - P_{O_{2,a}}) exp\left(\frac{RT\tau_{cathode}}{2FD_{eff,cathode}P} j\right) \tag{11}$$

In which $[D_{eff,anode}]$ (m^2s^{-1}) is effective gaseous diffusivity through the anode, and $[D_{eff,anode}]$ is the diffusivity through the anode (m^2s^{-1}), $[P_{H2,f}]$ and $[P_{H2O,f}]$ are the partial pressure in the fuel (bar). Similarly, $[P_{H2,TPB}]$, $[P_{O2,TPB}]$ and $[P_{H2O,TPB}]$ are the partial pressure (bar) in the three-phase boundary TPB. $[P]$ is the pressure in the SOFC (bar), and $[P_{O2,a}]$ the partial pressure in the air channel (bar). The $[F]$ is Faraday Constant $(Cmol^{-1})$ and $[\tau_{anode}]$ and $[\tau_{cathode}]$ are the thickness of the anode and cathode (μm).

The last irreversible loss to be calculated in the system is the activation loss, which is caused by the slow electrochemical reaction at the electrode surface. The activation loss, can be calculated using the Bulter-Volmer equation, as shown in following expression (12) and (13): (Saebea *et al.*, 2012).

$$j = j_{0,anode}\left[\frac{P_{H_2,TPB}}{P_{H_2,f}} exp\left(\frac{\alpha nF}{RT}\eta_{act,anode}\right) - \frac{P_{H_2O,TPB}}{P_{H_2O,f}} exp\left(-\frac{(1-\alpha)nF}{RT}\eta_{act,anode}\right)\right] \tag{12}$$

$$j = j_{0,cathode}\left[\frac{P_{H_2,TPB}}{P_{H_2,f}} exp\left(\frac{\alpha nF}{RT}\eta_{act,cathode}\right) - exp\left(-\frac{(1-\alpha)nF}{RT}\eta_{act,cathode}\right)\right] \tag{13}$$

where $[\alpha]$ is the transfer coefficient, $[n]$ is the number of electrons transferred. The $[n_{act,cathode}]$ and$[n_{act,anode}]$ are the activation overpotentials. The $[j_{0,anode}]$ and $[j_{0,cathode}]$ are the exchange current density at cathode and anode (V), expressed by the equations (14) and (15):

$$j_{0,anode} = \frac{RT}{nF} k_{anode} exp\left(-\frac{E_{anode}}{RT}\right) \tag{14}$$

$$j_{0,cathode} = \frac{RT}{nF} k_{cathode} exp\left(-\frac{E_{cathode}}{RT}\right) \tag{15}$$

Where $[E_{anode}]$ is activation energy of anode $(kJmol^{-1})$, and $[E_{cathode}]$ for cathode $(kJmol^{-1})$, and $[k_{anode}]$ and $[k_{cathode}]$ are pre-exponential factors of the anode (Am^{-2}), respectively. The electrical power output, $[P_{SOFC}]$ (kW), is the current flowing from the fuel cell times the actual voltage, as shown in the following equation (16):

$$P_{sofc} = A_c j V \tag{16}$$

The current density depends on hydrogen consumption in electrochemical reaction and area (Saebea *et al.*, 2012). Presented in the equation (17):

$$j = \frac{2F\dot{z}}{A_c} \tag{17}$$

In which $[\dot{z}]$ is the amount of hydrogen consumed in the reaction, $[A_c]$ the fuel cell active area *(m2)*, and F is the Faraday constant (C/mol).

The fuel utilization$[U_f]$, which relates to the amount of hydrogen consumed in the fuel cell reactions,$[\dot{z}]$, regarding to inlet components. This correlation is expressed by equation (18) (Saebea *et al.*, 2012).

$$U_f = \frac{\dot{z}}{(4\dot{n}_{CH4} + \dot{n}_{H2} + \dot{n}_{CO})} \tag{18}$$

3. REFORMER

SOFC may include a fuel reformer, which converts fuel into a hydrogen-rich gas. To provide the required hydrogen supply to the SOFC, cogeneration of the fuel through a reformer is an alternative. This equipment performs the decomposition of the fuel, into water and hydrogen, supplying the hydrogen to the fuel cell and releasing the water into the environment (Kupecki, 2018).

Inside the fuel reformer, ethanol, for example, can be converted to hydrogen through different catalytic reforming routes such as steam reforming, dry ethanol reforming, partial oxidation and autothermal ethanol reforming (Ma *et al.*, 2021). The autothermal method (oxidative steam reforming) is a combination of steam reforming and partial oxidation in a single process. This method is almost thermoneutral for ethanol reforming, presented in equation (19) (Tippawan and Arpornwichanop, 2014).

$$C_2H_5OH + xO_2 + (3-2x)H_2O \rightleftharpoons (6-2x)H_2 + 2CO_2 \tag{19}$$

The model of study considers the autothermic reforming process, in which the heat provided by the exothermic reaction in the SOFC can be recycled to provide heat to the endothermic reaction in the reformer.

To represent the reformer, it was assumed that the reformer is in the equilibrium state couple to the SOFC in the model implementation. As the reformer is in equilibrium state, is possible to use a function of the library Cantera to calculate the equilibrium. The function used is "Equilibrate" to minimize the total Gibbs Free energy of the mixture. The minimization of Gibbs free energy of a single phase system is given by the equation (19) (Oechsler *et al.*, 2020).

$$\dot{G}(\dot{n}_i, P, T) = \sum_{i=1}^{NC} \dot{n}_i \Delta G^o_{f_i} + RT \sum_{i=1}^{NC} (\dot{n}_i P) - RT \sum_{i=1}^{NC} \dot{n}_i \ln\left(\sum_{i=1}^{NC} \dot{n}_i\right) \tag{20}$$

where, $[\dot{G}_{fm,i}]$ is Formation Gibbs free energy of the chemical species, $[\dot{n}_i]$ is molar flow rate of chemical species i on outlet.

Thus, the objective is to find a molar flow set that minimizes Equation (19) with defined temperature and pressure, taking into account the mass balance constraints. It is convenient to formulate the mass balance constraints in terms of

elementary balances. If ak,i defines the total number of atoms of the kth element present in each chemical species i, while ni and ni0 represent the molar flow rate of chemical species i in the inlet and outlet streams, respectively, the mass balance for each element k can be written as:

The mass balances can be formulated as equation (26), where $[A_k]$ represents the total number of atomic weights, and $[a_{i_k}]$ is the total number of atoms. (Oechsler *et al.*, 2020)

$$\sum_{i=1}^{NC} a_{i,k}(\dot{n}_{io} - \dot{n}_i) = 0 \tag{21}$$

Therefore, the minimization of the total Gibbs free energy is calculated using the function using the Villars-Cruise-Smith (VCS) algorithm, detailed in the reference documentation (CANTERA, 2022).

In the literature, one can find different approaches to calculate the efficiency, however, the most observed in the papers are the thermodynamic efficiency and the electrical efficiency. The thermodynamic efficiency of a fuel cell is the ratio between the available electrical energy and useful energy of the fuel (Revankar and Majumdar, 2016), and electrical efficiency is the ratio between the available work in the fuel cell, and the reversible work, considering the major losses: activation, ohmic, and concentration loss (Revankar and Majumdar, 2016; O'Hayre *et al.*, 2016). This relation is given by equation (21), where $\eta_{electrical}$, is the electrical efficiency, E is open-circuit voltage *(V)*, and V the operating cell voltage *(V)*.

$$\eta_{electrical} = \frac{E}{V} \tag{22}$$

An important aspect of electrical efficiency is the dependence on current: the higher the current, the lower the voltage in the cell will be, resulting in low electrical efficiency. Therefore, a fuel cell is more efficient with low current (Revankar and Majumdar, 2016).

In addition to the efficiency calculated in terms of SOFC, the efficiencies in relation to the system can also be calculated. These relationships were used to evaluate the operating points of the system (Zhou *et al.*, 2022; Ma *et al.*, 2021; Saebea *et al.*, 2012). The electric efficiency,$\eta_{electricalsystem}$, is given by equation (22), as the relation of electric power to the enthalpy reaction of fuel (Zhou *et al.*, 2022).

$$\eta_{electrical,system} = \frac{P_{SOFC}}{m_{fuel} * LHV_{fuel}} \tag{23}$$

where, P_{SOFC}, is electric power of SOFC *(W)*, m_{fuel} is mass flow rate *(kg/s)* and LHV_{fuel} is lower heating value for the fuel *(kcal/Kg)*.

4. Methodology

The model was implemented using the Python language to represent the behavior of the solid oxide fuel cell (SOFC). This implementation was made using the library Cantera, and Numpy.

Cantera is an open-source library capable of solving different problems related with chemical kinetics, thermodynamic and transport phenomena (CANTERA, 2022). In this actual study, the function "equilibrate" was utilized with the ethanol file which simulates the properties of Ethanol, (Marinov, 1999) to represent the equilibrium state in the reformer. Once the equilibrium state is calculated, the output of the equilibrium function shows the species quantities, allowing to calculate the partial pressures which integrated with the SOFC model permit the representation of the component.

The parameters used to simulate the model and generate the results are detailed in Table 1 to achieve 5kW of nominal power. This configuration reaches the objective of power, but some other ranges of values have been studied during the process and the results are present in the next section. Values related to material conductivity and thickness were kept constant, and are detailed in Table 2.

Table 1. SOFC Parameters at nominal conditions

Description	**Parameter**	**Units**	**Value**
Temperature	T	(K)	973
Pressure	P	(atm)	1
Input Flow	m	(kg/s)	0.407
Ratio Ethanol/Water	-	(-)	3:1
Ratio Air/Ethanol	-	(-)	0.5
Fuel Utilization	Uf	-	0.7

Figure 2 presents a schematic of the SOFC system simulation, depicting the model blocks and their connections. The represented system has ethanol, water, and air as inputs, represented by streams 1, 4, and 7. Stream 1 supplies water to the evaporator (E01) where it is heated to the saturated steam temperature. The resulting steam then flows through line 2 to the next heat exchanger (HX001), where its temperature is further increased to 492°C. At the inlet of the mixer (M01), ethanol at 25°C and superheated water vapor. The stream 5 flow through heat exchanger (HX02) to be heated to 600°C, and fed the reformer (RE01). Subsequently, the ethanol is further heated to the desired temperature at the reformer inlet. The hydrogen-rich gas produced by the reformer is directed to the SOFC. Lastly, the exhaust from the SOFC is discharged through stream 12 and 13.

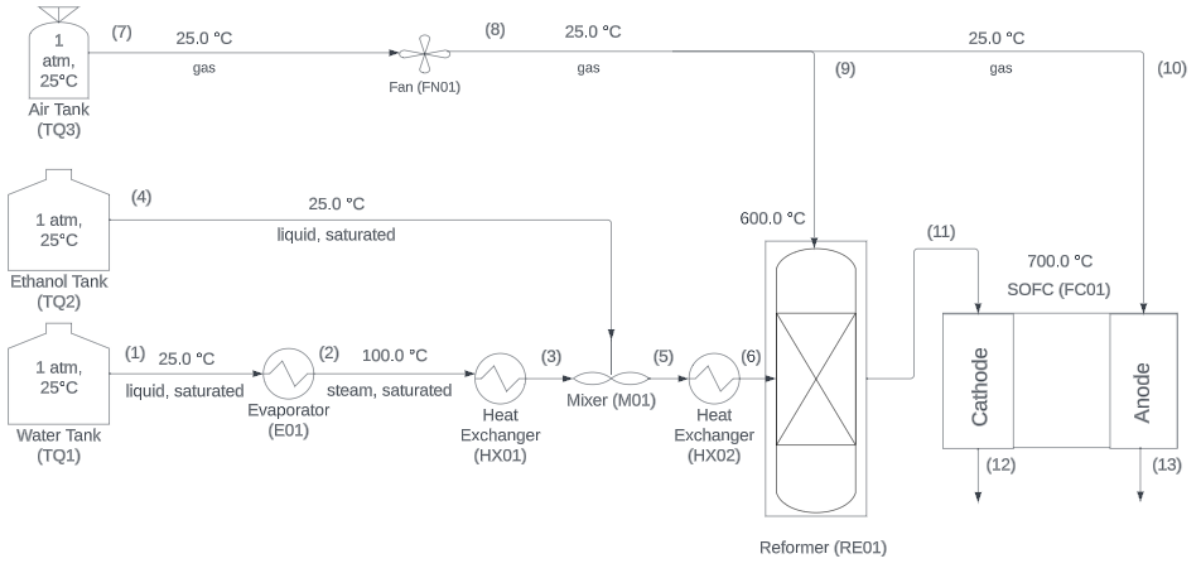

Figure 2. Schematic of SOFC System in Implementation: Block Diagram

The parameters in the diagram above are calculated separately so that it is possible to calculate the efficiency of the system in a non-recirculation condition. The representations of the heat exchangers were performed using the e-NTU method, verifying the heat and mass balances.

In this proposed diagram, the process flowsheet simulation is able to compute the heat transfer rates of the components, and thermal/electrical efficiencies. Furthermore, sensitivity analysis of model responses can be also performed, considering disturbances in flow rates, temperature, and air/ethanol and ethanol/water ratios. These simulations enable a comparison of the results with existing literature, allowing validate and assess the performance of the system under varying conditions

Table 2. Constant parameter during simulation

Description	**Units**	**Value**
Pre-exponential factor of anode exchange current density,	A m^{-2}	6.54×10^{11}
Pre-exponential factor of cathode exchange current density	A m^{-2}	2.35×10^{11}
Activation energy of anode exchange current density	kJ mol^{-1}	140
Activation energy of cathode exchange current density	kJ mol^{-1}	137
Anode diffusion coefficient	$m^2 s^{-1}$	3.66×10^{-5}
Cathode diffusion coefficient	$m^2 s^{-1}$	1.37×10^{-5}
Anode electrical conductivity	$\Omega^{-1} m^{-1}$	$4.2{\times}10^7 exp(\frac{-1200}{T})$
Cathode electrical conductivity	$\Omega^{-1} m^{-1}$	$9.5{\times}10^7 exp(\frac{-1200}{T})$
Electrolyte ionic conductivity	$\Omega^{-1} m^{-1}$	$33.4 \times 10^3 exp(\frac{-10300}{T})$
Anode thickness	μm	500
Cathode thickness	μm	50
Electrolyte thickness	μm	20

Source:(Saebea et al.*, 2012).*

5. RESULTS AND DISCUSSIONS

To validate the results obtained from the model, it is highly advisable to consult the literature reference and the experimental data. The values obtained from the SOFC model simulation can be compared to the corresponding experimental results cited in the published works at temperatures of 873K and 1073K, as can be seen in Figure 3 (Saebea *et al.*, 2012; Zhang *et al.*, 2010).

Figure 3 presents the simulated results of the voltage obtained from the model in comparison with the experimental results. The blue dots represent the value at a temperature of 873 K. When compared to the identity line, it shows a correlation between the model and the experimental results. At some degree, it is perceived that there is a slight deviation from the identity line, although this is also observed in the reference model. The orange dots represent the points at temperature 1073 K, which show a better correlation than 873K, which at some degree even touched the identity line. When the voltage goes higher than 0.9, the distance is farther from the identity line, indicating less correlation in comparison to using the range 0.4 to 0.8 volts.

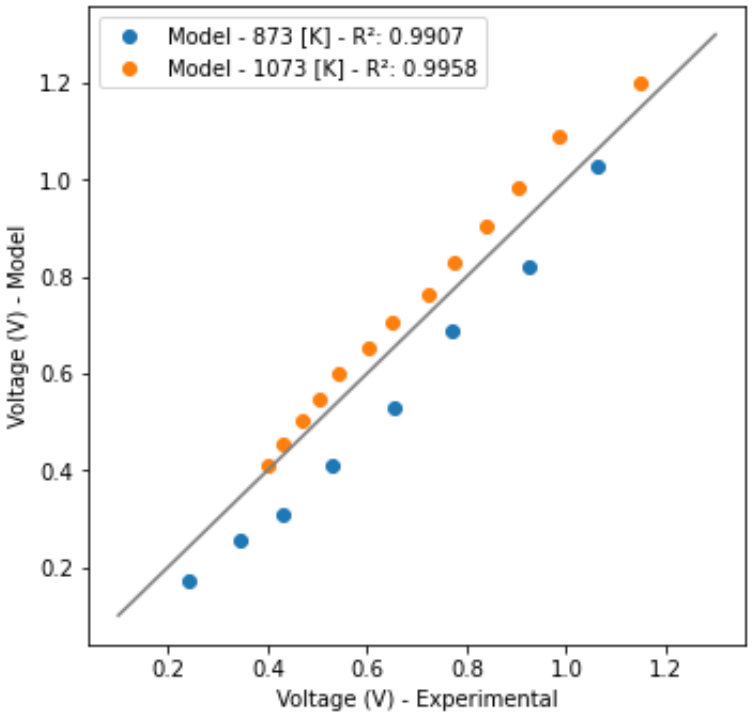

Figure 3. The comparison between Voltage and model predictions and experimental voltage results at temperatures of 873 and 1073 *(K)*

Through the implemented model, simulations were carried out with the objective of exploring the characteristics of the model and understanding the effect of some parameters of interest. Figure 4 summarizes some studies carried out with the variation of design parameters such as air/ethanol ratio and temperature. On the left side are represented the impacts related to the temperature, and the ratio air/ethanol.

One of the objectives of this work is to obtain the design parameters for the cell power to reach approximately 5kW. When the inlet flow rate is increased in a system, it is generally expected to result in an increase in power output. However, it is worth noting that in certain cases, particularly with solid oxide fuel cells (SOFCs), increasing the flow rate can lead to a decrease in the SOFC voltage.(O'Hayre *et al.*, 2016).

This phenomenon can occur due to several reasons. Higher flow rates can provide a higher rate of reactant supplied to the SOFC, which can lead to an increase in the concentration overpotential. This overpotential arises from the limitations in the rate at which reactants can be consumed at the electrode surfaces. Additionally, increasing the flow rate can also result in a higher pressure drop across the fuel cell system, decreasing the overall eficiency. These losses can contribute to a decrease in the SOFC voltage . This voltage decay is explained by the increase in current density, which consequently increases ohmic losses, due to activation and concentration.

Indeed, air/ethanol ratio can have a significant impact on the power output of the system. An increase in the air/ethanol ratio generally leads to a decrease in power generation. This effect can be attributed to the stoichiometry of the autothermal reforming reaction of ethanol. In this reaction, an excess of air (oxygen) compared to the stoichiometric requirement for complete combustion can result in the formation of more carbon dioxide (CO2) rather than hydrogen (H2), as can be seen in chemical equation (3). Since the generation of hydrogen is essential for power production in an SOFC, an increased

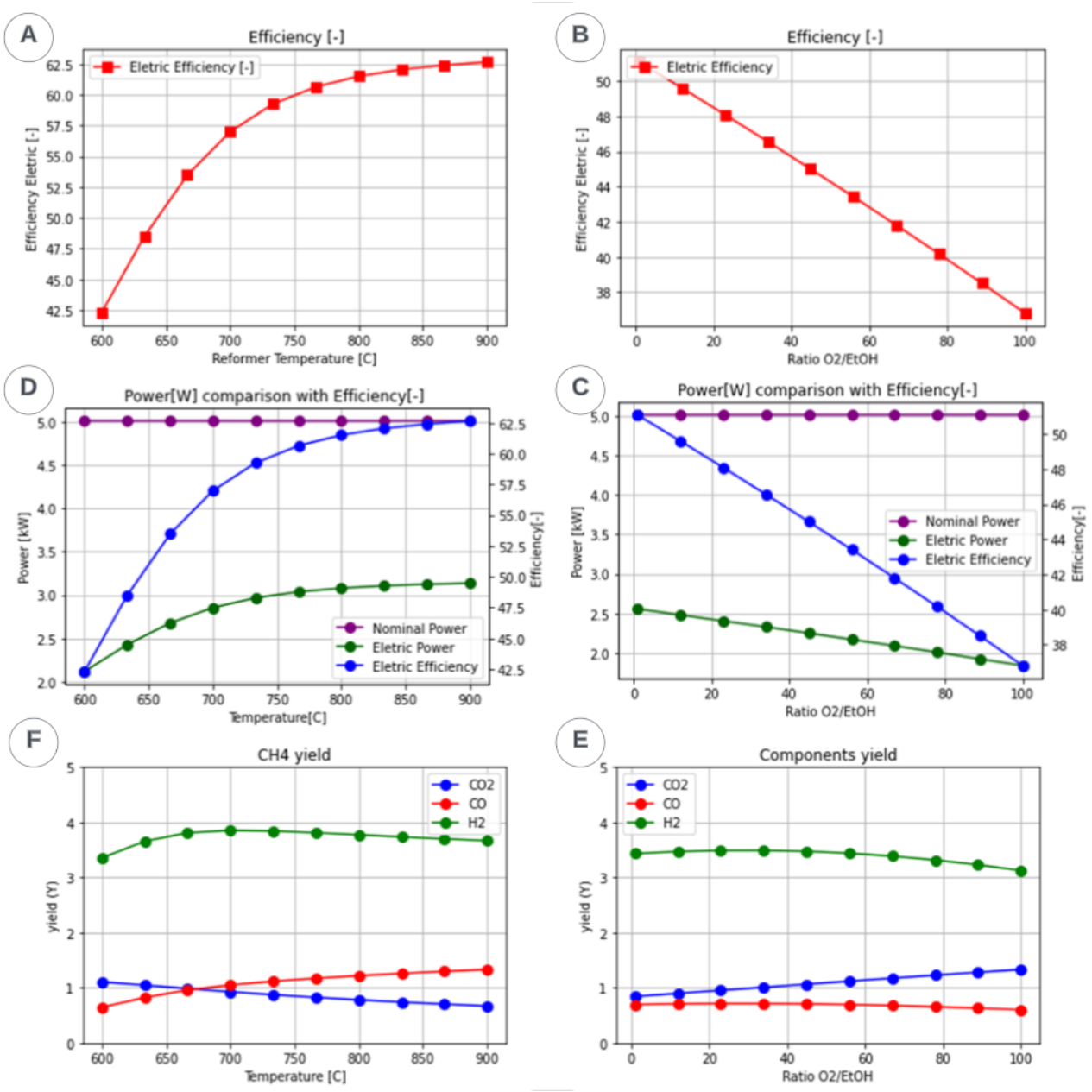

Figure 4. Effect of temperature and O2/EtOH Ratio in Efficiencies and Reformer Heatload

air/ethanol ratio can lead to a lower hydrogen yield (as can be seen in Figure 4e), reducing the power output (Figure 4c).

In addition, the air/ethanol ratio increase not only affects the power output but also influences the nature of the reforming reaction, shifting it from endothermic to exothermic. The exothermic nature of the reforming reaction at higher air/ethanol ratios opens up the possibility of supplying heat to the system. Instead of relying solely on external heat sources, the excess heat generated from the exothermic reaction can be utilized within the system. This behavior is observed in Figure 4 left. However, as pointed out the increase of air/ethanol also decreases the efficiency of the system. On the other hand is possible to see that the temperature variation can impact the efficiency, which combined with the input ratio can help to be a trade-off to the model.

Besides, in the right of Figure 4 the effect in the yield of components for the variation of O2/EtOH ratio after the chemical equilibrium. The model correctly predicts the behavior for a SOFC cell, as well as for a reformer, allowing to carry out studies in order to address the issues raised as the objective of the work. It is possible to say that there are points that satisfy the power conditions required by the system and that this work adds to the analysis of the system working with the heat supplied only by the reformer.

Another parameter that causes an impact on in power is the air/ethanol ratio, wherein the increase causes a decrease in power, which can be seen in the stoichiometry of the autothermal reforming reaction of ethanol. In addition, varying the air/ethanol ratio alters the behavior of ethanol reforming from endothermic to exothermic, allowing discuss the possibility

of supplying heat to the system. This behavior is observed in Figure 4.a, in which the variation of Air/Ethanol causes a decrease in the efficiency of the system. On the other hand is possible to see that the temperature variation can impact the electrical efficiency of the system, observed in the sub-figure 4.b.

Figure 4.e shows the effect of temperature variation in the yields of CO2, CO and H2. Despite the variation of 300°C in temperature, the formation of H2 does not change much. The yield of H2 for the variation of ratio O2/EtOH has more noticeable, as for the CO2, and CO yield.

Lastly, the impact of temperature variation in the SOFC Electrical Power and nominal is present in Figure 4.d. The blue line, shows the efficiency result, with impact caused by the variation of electrical power variation. The nominal power is not impacting as it is direct relation of mass flow rate to the low heat value of ethanol (LHV). In Figure 4.c, the same study was conducted but compared the impact of variation of O2/Ethanol, presenting a reduction of efficiency due to the increase of O2 in the system.

6. CONCLUSION

The implementation of the model presented satisfactory results in the representation of the SOFC behavior, even though there are many hypotheses for simplifying the model. It is possible to observe that the lumped model fulfills the role of anticipating the impact of the effect of the sensitivity of important characteristics, allowing to save test time in the laboratory. The use of the Cantera library helps the implementation and opens opportunities to test the same model with many options of Fuel.

The results indicates that for the condition of 5kW nominal power, the efficiencies can variate from 42.5% to 62.5% within a range of 300°C in temperature. A similar investigation for air/ethanol ratio was conducted and provided a efficiency result of 51% to 37%, as the proportion of air/ethanol increases. An observation of the model's equations shows how dependent on the temperature the model is, which results in the temperature being a key parameter in the results. However, the impact of variation in the ratio of Oxygen/Water is very representative as it permits the system to move from an endothermic to an exothermic condition. This point leads to important discussions about possible trade-offs depending on the size of the system, as well the utilization and Fuel.

7. REFERENCES

Alhazmi, N., Almutairi, G., Alenazey, F. and AlOtaibi, B., 2021. "Three-dimensional computational fluid dynamics modeling of button solid oxide fuel cell". *Electrochimica Acta*, Vol. 390. ISSN 00134686. doi:10.1016/j.electacta.2021.138838.

Arpornwichanop, A., Chalermpanchai, N., Patcharavorachot, Y., Assabumrungrat, S. and Tade, M., 2009. "Performance of an anode-supported solid oxide fuel cell with direct-internal reforming of ethanol". *International Journal of Hydrogen Energy*, Vol. 34, No. 18, pp. 7780–7788. doi:10.1016/j.ijhydene.2009.07.006. URL `https://doi.org/10.1016/j.ijhydene.2009.07.006`.

Badur, J., Lemański, M., Kowalczyk, T., Ziółkowski, P. and Kornet, S., 2018. "Zero-dimensional robust model of an sofc with internal reforming for hybrid energy cycles". *Energy*, Vol. 158. ISSN 03605442. doi:10.1016/j.energy.2018.05.203.

BioDieselbr, 2006. "Próalcool - programa brasileiro de álcool". URL `https://www.biodieselbr.com/proalcool/pro-alcool/programa-etanol#:~:text`.

CANTERA, 2022. "Cantera properties". URL `https://cantera.org/documentation/docs-2.6/sphinx/html/cython/thermo.html?highlight=equilibrate#cantera.Mixture.equilibrate`.

Cheddie, D.F. and Munroe, N.D., 2007. "A dynamic 1d model of a solid oxide fuel cell for real time simulation". *Journal of Power Sources*, Vol. 171. ISSN 03787753. doi:10.1016/j.jpowsour.2007.06.170.

Chen, X., Pan, Y. and Chen, J., 2010. "Performance and evaluation of a fuel cell-thermoelectric generator hybrid system". *Fuel Cells*, Vol. 10. ISSN 16156846. doi:10.1002/fuce.200900208.

FAPESP, A., 2016. "Proálcool: Uma das maiores realizações do brasil baseadas em ciência e tecnologia". https://agencia.fapesp.br/proalcool-uma-das-maiores-realizacoes-do-brasil-baseadas-em-ciencia-e-tecnologia/24432/.

Kaczmarczyk, R. and Gurgul, S., 2021. "A thermodynamic analysis of heavy hydrocarbons reforming for solid oxide fuel cell application as a part of hybrid energy systems". *Energies*, Vol. 14. ISSN 1996-1073. doi:10.3390/en14020337.

KELES, D., WIETSCHEL, M., MOST, D. and RENTZ, O., 2008. "Market penetration of fuel cell vehicles – analysis based on agent behaviour". *International Journal of Hydrogen Energy*, Vol. 33, No. 16, pp. 4444–4455. doi:10.1016/j.ijhydene.2008.04.061. URL `https://doi.org/10.1016/j.ijhydene.2008.04.061`.

Kupecki, J., ed., 2018. *Modeling, Design, Construction, and Operation of Power Generators with Solid Oxide Fuel Cells*. Springer International Publishing. ISBN 978-3-319-75601-1. doi:10.1007/978-3-319-75602-8.

Ma, S., Lin, M., Lin, T.E., Lan, T., Liao, X., Maréchal, F., herle, J.V., Yang, Y., Dong, C. and Wang, L., 2021. "Fuel cell-battery hybrid systems for mobility and off-grid applications: A review". *Renewable and Sustainable Energy Reviews*, Vol. 135. ISSN 13640321. doi:10.1016/j.rser.2020.110119.

Marinov, N.M., 1999. "A detailed chemical kinetic model for high temperature ethanol oxidation". *International Journal of Chemical Kinetics*, Vol. 31, No. 3, pp. 183–220. doi:10.1002/(sici)1097-4601(1999)31:3<183::aid-kin3>3.0.co;2-x. URL https://doi.org/10.1002/(sici)1097-4601(1999)31:3<183::aid-kin3>3.0.co;2-x.

Nissan, 2016. "Nissan unveils world's first solid-oxide fuel cell vehicle". URL https://global.nissannews.com/en/releases/nissan-unveils-worlds-first-solid-oxide-fuel-cell-vehicle.

Oechsler, B.F., Lima, R.C., Dutra, J.C.S., Bittencourt, R.C.P. and Pinto, J.C., 2020. "Analysis and simulation of catalytic steam prereforming of hydrocarbons in adiabatic tubular reactors". *Industrial &amp Engineering Chemistry Research*, Vol. 59, No. 46, pp. 20285–20297. doi:10.1021/acs.iecr.0c03524. URL https://doi.org/10.1021/acs.iecr.0c03524.

O'Hayre, R., Cha, S.W., Colella, W. and Prinz, F.B., 2016. *Fuel Cell Fundamentals*. John Wiley Sons, Inc. ISBN 9781119191766. doi:10.1002/9781119191766.

Revankar, S.T. and Majumdar, P., 2016. *Fuel Cells*. CRC Press. doi:10.1201/b15965. URL https://doi.org/10.1201/b15965.

Saebea, D., Patcharavorachot, Y. and Arpornwichanop, A., 2012. "Analysis of an ethanol-fuelled solid oxide fuel cell system using partial anode exhaust gas recirculation". *Journal of Power Sources*, Vol. 208. ISSN 03787753. doi:10.1016/j.jpowsour.2012.02.023.

Tippawan, P. and Arpornwichanop, A., 2014. "Energy and exergy analysis of an ethanol reforming process for solid oxide fuel cell applications". *Bioresource Technology*, Vol. 157. ISSN 09608524. doi:10.1016/j.biortech.2014.01.113.

Wang, K., Hissel, D., Péra, M., Steiner, N., Marra, D., Sorrentino, M., Pianese, C., Monteverde, M., Cardone, P. and Saarinen, J., 2011. "A review on solid oxide fuel cell models". *International Journal of Hydrogen Energy*, Vol. 36. ISSN 03603199. doi:10.1016/j.ijhydene.2011.03.051.

Yang, B., Wang, J., Zhang, M., Shu, H., Yu, T., Zhang, X., Yao, W. and Sun, L., 2020. "A state-of-the-art survey of solid oxide fuel cell parameter identification: Modelling, methodology, and perspectives". *Energy Conversion and Management*, Vol. 213. ISSN 01968904. doi:10.1016/j.enconman.2020.112856.

Zhang, X., Chan, S., Li, G., Ho, H., Li, J. and Feng, Z., 2010. "A review of integration strategies for solid oxide fuel cells". *Journal of Power Sources*, Vol. 195. ISSN 03787753. doi:10.1016/j.jpowsour.2009.07.045.

Zhao, H. and Burke, A.F., 2009. "Optimization of fuel cell system operating conditions for fuel cell vehicles". *Journal of Power Sources*, Vol. 186. ISSN 03787753. doi:10.1016/j.jpowsour.2008.10.032.

Zhou, J., Wang, Z., Han, M., Sun, Z. and Sun, K., 2022. "Optimization of a 30 kW SOFC combined heat and power system with different cycles and hydrocarbon fuels". *International Journal of Hydrogen Energy*, Vol. 47, No. 6, pp. 4109–4119. doi:10.1016/j.ijhydene.2021.11.049. URL https://doi.org/10.1016/j.ijhydene.2021.11.049.

8. RESPONSIBILITY NOTICE

The following text, properly adapted to the number of authors, must be included in the last section of the paper: The author(s) is (are) solely responsible for the printed material included in this paper.